

Journal of Materials Chemistry A

Accepted Manuscript



This is an *Accepted Manuscript*, which has been through the Royal Society of Chemistry peer review process and has been accepted for publication.

Accepted Manuscripts are published online shortly after acceptance, before technical editing, formatting and proof reading. Using this free service, authors can make their results available to the community, in citable form, before we publish the edited article. We will replace this *Accepted Manuscript* with the edited and formatted *Advance Article* as soon as it is available.

You can find more information about *Accepted Manuscripts* in the [Information for Authors](#).

Please note that technical editing may introduce minor changes to the text and/or graphics, which may alter content. The journal's standard [Terms & Conditions](#) and the [Ethical guidelines](#) still apply. In no event shall the Royal Society of Chemistry be held responsible for any errors or omissions in this *Accepted Manuscript* or any consequences arising from the use of any information it contains.

1 **Interconnected Three-Dimensional V₂O₅/Polypyrrole Network** 2 **Nanostructures for High Performance Solid-State** 3 **Supercapacitors**

4
5 Tao Qian,[†] Na Xu,[†] Jinqiu Zhou, Tingzhou Yang, Xuejun Liu, Xiaowei Shen, Jiaqi Liang,
6 and Chenglin Yan*

7
8 Dr. Tao Qian, Na Xu, Jinqiu Zhou, Tingzhou Yang, Xuejun Liu, Xiaowei Shen, Jiaqi Liang,
9 Prof. Dr. Chenglin Yan

10 College of Physics, Optoelectronics and Energy & Collaborative Innovation Center of Suzhou
11 Nano Science and Technology, Soochow University, Suzhou 215006, China. [†]The first two
12 authors contributed equally to this work. Email: c.yan@suda.edu.cn

14 **Abstract**

15
16 *Supercapacitor electrodes composed of 3D V₂O₅ network with polypyrrole (PPy) uniformly*
17 *decorated onto each nanowire were fabricated to enhance their pseudocapacitive*
18 *performance. The continuous 3D network creates channels for better ion transport, and the*
19 *high degree of pore connectivity in the network enhances the mass transport. The PPy shell*
20 *could enhance electric conductivity and prevent the dissolution of vanadium. These merits*
21 *together with the ideal synergy between V₂O₅ and PPy lead to high specific capacitance of*
22 *448 F g⁻¹, which is three times higher than that of the stacked V₂O₅. The all-solid-state*
23 *symmetric supercapacitor device assembled by V₂O₅/PPy core/shell 3D network exhibits high*
24 *energy density (14.2 Wh kg⁻¹) at a power density of 250 W kg⁻¹ and good cyclic stability*
25 *(capacitance retention of 81% after 1000 cycles). Furthermore, the prepared device could*
26 *power a red light-emitting diode indicator efficiently after charging for only 10 s.*

27

28

1 Introduction

2 Supercapacitors, also called electrochemical capacitors or ultracapacitors, are a class of
3 electrochemical energy storage devices exhibiting high power density, long cycling life, and
4 excellent reversibility.¹⁻⁴ Supercapacitors can be classified into two types based on their
5 charge-storage mechanism: double layer capacitors with carbon electrodes and
6 pseudocapacitors with metal oxide or conducting polymer electrodes.⁵⁻⁶ For pseudocapacitors,
7 properties such as high specific surface area, high electrical conductivity and fast diffusion
8 properties are important to achieve high power density and energy density. Transition-metal
9 oxides such as RuO₂,⁷ MnO₂,⁸ Co₃O₄,⁹ NiO,¹⁰ and V₂O₅¹¹⁻¹² have higher capacity than
10 electrochemical double-layer capacitive carbon materials due to their unique redox reaction.
11 Among various transition-metal oxides, V₂O₅ possesses the advantages of high energy
12 density,¹³ natural abundance, low cost, unique layered structures and wide potential window
13 arising from its various vanadium oxidation states (V²⁺, V³⁺, V⁴⁺, and V⁵⁺).¹⁴ Many efforts
14 have been done to fabricate different nanostructures of V₂O₅ such as nanoribbons,¹⁵
15 nanotubes,¹⁶ nanorods,¹⁷ nanosheets,¹⁸ and nanowires,¹⁹ which have been demonstrated
16 effective to improve the performance of V₂O₅-based supercapacitors. However, the problems
17 of V₂O₅'s poor structural stability (due to the V₂O₅ dissolution in the aqueous electrolyte),
18 low conductivity and slow electrochemical kinetics which limit specific capacity and long-
19 term cycling stability have not been solved well.²⁰⁻²¹

20

21 On the other hand, combining V₂O₅ with carbon materials has been justified to be an effective
22 method to improve electric transport properties of V₂O₅,^{6, 22} but the cyclic stability is still
23 undesirable because such combination cannot prevent the dissolution of vanadium which
24 leads to the loss of active materials. Polypyrrole (PPy) is an intrinsically conductive polymer
25 as pseudocapacitor material because of its high conductivity, storage ability, redox and
26 capacitive current and good thermal and environmental stability.²³⁻²⁵ To solve above issues, in

1 the current work, we have developed interconnected 3D V_2O_5 network nanostructures
2 constructed through a “seeding approach” by Ni substrate, which can afford to drastically
3 optimize the morphology of the as-produced V_2O_5 . The prepared V_2O_5 then promoted the in
4 situ polymerization process by oxidizing the pyrrole monomer into 3D network forms, and
5 obtained V_2O_5 /PPy interconnected core-shell structures. The continuous 3D network creates
6 channels for better ion transport to the redox-active material, and the high degree of pore
7 connectivity in the network enhances the mass transport as well as increases the material
8 lifetime of the device. The decorated PPy shell simultaneously utilizes the high electronic
9 conductivity of PPy with respect to that of V_2O_5 , and polymeric coating effect of PPy to
10 prevent the dissolution of vanadium. As a result, the 3D V_2O_5 /PPy core/shell network exhibits
11 remarkably enhanced specific capacitance of 448 F g^{-1} , which is over three times higher than
12 that of the stacked V_2O_5 nanostructures. The improved capacitance retention of 81% was
13 maintained after 1000 cycles, which is better than those of the reported V_2O_5 nanowires,
14 nanotubes, and nanoflowers.

15

16 **Experimental Section**

17 *Synthesis of V_2O_5 network nanostructures*

18 60 mL sodium metavanadate solution (1 M) was dropped onto Ni substrate through ion-
19 exchange column, then standing for overnight. The products were collected by centrifugation
20 and crystallization at $400 \text{ }^\circ\text{C}$ for 2h.

21

22 *Synthesis of V_2O_5 /PPy core/shell network nanostructures*

23 10 μL hydrogen peroxide (30 wt %) was added to the mixture of 50 mg as-prepared V_2O_5
24 network, 5 μL pyrrole, and 10 mL deionized water. The PPy shell could decorate on the
25 porous V_2O_5 network uniformly after 12 h vigorously stirring.

26

27 *Structure Characterization*

28 The morphology of the nanostructures was investigated by field emission scanning electron
29 microscopy (FESEM, SU8010, Japan), and field emission transmission electron microscopy

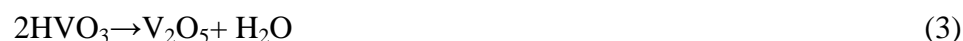
(FETEM, FEI Tecnai G220, America). Surface elemental analysis was performed on x-ray photoelectron spectrometer (XPS, Kratos Axis Ultra Dld, Japan).

Electrochemical Characterization

Electrochemical tests were carried out using CHI 660E (Chenhua Shanghai, China) electrochemical workstation. The working electrodes were prepared by making slurry of 70 wt % active materials, 20 wt % acetylene black, and 10 wt % polytetrafluoroethylene (PTFE, 60 wt % dispersion in water) in ethanol. The obtained slurry was then coated onto titanium foil as current collector within an area of $1 \times 3 \text{ cm}^2$ and areal mass of 0.25 mg cm^{-2} , which were then dried in vacuum at $60 \text{ }^\circ\text{C}$ for 12 h to remove the solvent. Cyclic voltammetry (CV), charge-discharge and electrochemical impedance spectroscopy (EIS) were measured in three-electrode and two-electrode system, respectively. In half-cell tests, a three-electrode system was used to measure the response of the $\text{V}_2\text{O}_5/\text{PPy}$ network, where the prepared electrode was served as working electrode using 5 M LiNO_3 aqueous solution as the electrolyte, with Pt mesh as the counter electrode and Ag/AgCl as the reference electrode. In full cell tests, the supercapacitor was assembled to measure the device performance. In detail, LiNO_3/PVA (Polyvinyl Alcohol) gel electrolyte was prepared as follows: 6.9 g of LiNO_3 and 3 g of PVA were added into 20 mL of deionized water, and then the whole mixture was heated to $90 \text{ }^\circ\text{C}$ under stirring until the solution became clear. To assemble solid-state symmetric supercapacitor, two pieces of the prepared electrodes were assembled with a $\sim 120 \text{ }\mu\text{m}$ thick membrane (DR2012, Suzhou Beige New Materials & Technology Co. Ltd.) saturated with LiNO_3/PVA gel as the separator, sandwiched in between (Fig. 4A). The total thickness of the devices was less than 0.4 mm.

Results and discussion

The fabrication technique essentially consists of two parts (Fig. S1). Firstly, V_2O_5 network was synthesized through “seeding approach” with Ni substrate, the reaction process can be expressed as:



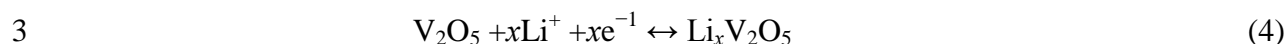
1 where the step (1) illustrates the “seeds” are obtained by double hydrolysis of $\text{Ni}(\text{VO}_3)_2$; step
2 (3) reveals the grown process of V_2O_5 which occupied the main component of network.
3 Secondly, the pyrrole monomer was polymerized into the 3D network formation by oxidizing.
4
5 To investigate the morphology of the fabricated 3D V_2O_5 /PPy core/shell network, scanning
6 electron microscopy (SEM) and transmission electron microscopy (TEM) images were
7 carried out and results are shown in Fig. 1. It is apparent that the 3D V_2O_5 network can be
8 constructed through “seeding approach” (Fig. 1A). The magnified SEM image (Fig. 1B)
9 further reveals the detailed morphology of the V_2O_5 network which is composed of nanowires.
10 The SEM image of the V_2O_5 /PPy core/shell network given in Fig. 1C illustrates that the
11 integration of PPy into the network does not deteriorate the ordered structure. TEM images
12 (Fig. 1D) of the V_2O_5 /PPy network further prove that core/shell structures with the PPy film
13 uniformly formed on the V_2O_5 nanowire surface are obtained. Inset shows the amorphous PPy
14 shell structures and inner V_2O_5 crystalline structures with a lattice spacing of 0.44 nm in detail.
15
16 X-ray photoelectron spectroscopy (XPS) spectra of the V_2O_5 and V_2O_5 /PPy network were
17 investigated as shown in Fig. 2A. In the survey region from 200 to 900 eV, it is evident that V,
18 O, and Ni elements all exist in the sample of V_2O_5 network before PPy coating. From careful
19 inspection of wide region spectroscopy and elemental analysis, it could be observed that for
20 V_2O_5 /PPy hybrid network, the peak of N1s appears at 399.57 eV (also shown in Fig. 2B) and
21 the peak intensity of C1s at 284.42 eV is enhanced, which both indicate the existence of PPy.
22 Fig. 2C and D reveal the high-resolution spectrum of V and Ni for the V_2O_5 /PPy hybrid
23 network. The two peaks were assigned to $\text{V}2\text{p}_{3/2}$ and $\text{V}2\text{p}_{1/2}$ at the binding energy of 516.72
24 eV and 524.57 eV, respectively (Fig. 2C), implying the formation of V_2O_5 phase in the
25 nanocomposite matrix.^{5, 15} From Fig. 2D, the only one peak at 855.32 eV corresponding to
26 Ni2p was observed, which justifies the presence of $\text{Ni}(\text{OH})_2$.²⁶ These results demonstrate that

1 V_2O_5 network was successfully fabricated by seeding of Ni substrate and coating it with PPy
2 shell.

3
4 To explore the potential application of the electrode material for supercapacitor, CV curves of
5 the stacked V_2O_5 , V_2O_5 network, and V_2O_5 /PPy core/shell network at different scan rates are
6 shown in Fig. S2A, B, and C, respectively. All of the figures show well-resolved two pairs of
7 cathodic and anodic peaks which are very distinct from those of the electric double-layer
8 capacitance in which the curve shape is normally close to ideal rectangular shape, and the
9 current of the electrode responses quasi-linearly with increasing potential scan rate,
10 demonstrating its excellent reactivity.²⁷ Comparison among three different electrode materials
11 is demonstrated by CV curves at a scan rate of 100 mV s^{-1} in Fig. S2D. For V_2O_5 network,
12 cathodic and anodic peaks could be distinguished much more obviously in contrast to that of
13 the stacked V_2O_5 , such network structure with ultrafine wires and multilevel pores is
14 favorable for providing easy access of the electrolyte to the materials and large electroactive
15 surface that is advantageous in energy storage applications.²⁸ However, the CV curve of the
16 V_2O_5 /PPy core/shell network expands distinctly with larger integral area in comparison with
17 that of V_2O_5 network, certifying the preferable capacitor performance attributable to the
18 improved electronic conductivity of the nanocomposite derived from PPy coating. The above
19 phenomena demonstrate that V_2O_5 network coated with PPy shell exhibits remarkable
20 electrochemical performance for supercapacitor electrodes.

21
22 Galvanostatic charge/discharge experiments at different current densities were performed to
23 estimate the specific capacitance of the stacked V_2O_5 , V_2O_5 network, and V_2O_5 /PPy core/shell
24 network as supercapacitor electrodes (Fig. 3A, B, and C). Two well-defined plateaus during
25 the discharge processes are observed in all of the figures revealing their satisfactory pseudo-

1 capacitive behavior. The electrochemical Li^+ insertion process occurring at V_2O_5 electrodes
2 can be expressed as:



4 where x is the mole fraction of inserted Li^+ ions. The typical galvanostatic charge/discharge
5 curves of stacked V_2O_5 , V_2O_5 network, and $\text{V}_2\text{O}_5/\text{PPy}$ core/shell network measured at a
6 current density of 0.5 A g^{-1} are shown in Fig. 3D for comparison. The two discharge plateaus
7 of $\text{V}_2\text{O}_5/\text{PPy}$ core/shell network are much distinguished and the discharge time is much larger
8 than that of the stacked V_2O_5 and V_2O_5 network, demonstrating higher electrochemical
9 activity behavior. Furthermore, the specific capacitance (C_m) of the device is calculated by the
10 following equation:

$$11 \quad C_m = I\Delta t/m\Delta E \quad (5)$$

12 where I is the discharge current, Δt is the discharge time, ΔE is the potential window during
13 the discharge process, and m is the effective electrode mass.²⁹ In case of $\text{V}_2\text{O}_5/\text{PPy}$ core/shell
14 network, a high specific capacitance of 448 F g^{-1} is obtained at a current density of 0.5 A g^{-1}
15 which is much higher than those of V_2O_5 network (318.5 F g^{-1}) and stacked V_2O_5 (143 F g^{-1})
16 at the same testing conditions (Fig. 3E). These results demonstrate that the 3D network
17 structure with PPy shell is preferable to improve the capacitive performance of V_2O_5 base-
18 materials.

19
20 EIS measurement in the frequency range of 10 mHz to 1000 kHz was performed to clearly
21 understand the ion diffusion of the electrodes (Fig. 3F). The Nyquist plots of the electrodes all
22 show the form with semicircle at higher frequency region and spike at lower frequency which
23 is the characteristic of the capacitive behavior. Ohmic resistance of the electrolyte and the
24 electrode materials is denoted as R_s , which is the intersection of the curve at the real part. The
25 interfacial charge transfer resistance (R_{CT}) is connected to represent the semicircle in the high
26 frequency region.³⁰ For the V_2O_5 network electrode, it shows the same R_s ($\sim 1.65 \text{ } \Omega$) and the

1 smaller R_{CT} ($\sim 0.8 \Omega$) compared with those of stacked V_2O_5 ($R_{CT} \sim 7 \Omega$) because the network
2 structure is beneficial to accelerate the charge transfer. In case of V_2O_5/PPy core/shell
3 network, R_S is only $\sim 1.09 \Omega$, which is much lower than that of V_2O_5 network ($\sim 1.65 \Omega$)
4 electrodes, clearly demonstrating the high conductivity after PPy coating. However, the R_{CT}
5 ($\sim 3.5 \Omega$) is relatively larger than that of V_2O_5 network, which is attributed to the inhibition for
6 the charge transfer of the PPy coating.

7
8 To further explore the advantages of the prepared materials for real applications, the
9 symmetric supercapacitor was assembled from two pieces of 3D V_2O_5/PPy core/shell network,
10 each with a mass loading of 0.75 mg, as shown in Fig. 4A. Fig. 4B shows the CV curves in
11 the potential window between 0 and 1 V, which present essentially the same nearly
12 rectangular shape as the scan rate increases from 5 to 100 $mV s^{-1}$, indicating the good
13 capacitive behavior of the device. Furthermore, the charge/discharge curves are similar in
14 shape between 0 and 1 V at different current densities from 0.5 to 10 $A g^{-1}$ (Fig. 4C),
15 illustrating that the supercapacitor can be stably performed in a wide range of current
16 densities. Nyquist plots of the symmetric supercapacitor were carried out (as shown in Fig.
17 S3), which reveal the same R_S ($\sim 1.09 \Omega$) and higher R_{CT} ($\sim 8.5 \Omega$), as compared with those of
18 the prepared electrode in aqueous electrolyte. The main reason is due to the fact that the gel
19 electrolyte and diaphragm take disadvantage of the charge transfer between the electrodes.

20
21 Ragone plots of the device describing the relationship between energy density and power
22 density were obtained, which is shown in Fig. 4D. The power densities and energy densities
23 of the symmetric supercapacitor performed in this work were collected to compare with the
24 values reported for other metal oxide-based supercapacitor devices. The Ragone plots show
25 that the energy density and power density of the prepared device are considerably higher than
26 those of metal oxide-based supercapacitor devices. Moreover, the supercapacitor also keeps

1 excellent rate behavior, with energy density of 10.14 Wh kg^{-1} at a power density of 5000 W
2 kg^{-1} .

3
4 We fabricated symmetric supercapacitors based on the as-prepared $\text{V}_2\text{O}_5/\text{PPy}$ core/shell
5 network and investigated their cycling stability in both 5 M LiNO_3 aqueous solution and
6 LiNO_3/PVA gel electrolyte. Fig. 4E illustrates the specific capacitance retention as a function
7 of cycle number, the capacitance of $\text{V}_2\text{O}_5/\text{PPy}$ core/shell network electrode decreases
8 continuously in aqueous solution, and only about 5.7% of the initial capacitance is retained
9 after 1000 cycles. The poor cycling performance of electrodes is mainly due to the instability
10 of V_2O_5 in aqueous electrolyte and the ease of the formation of highly soluble complexes.^{31,32}
11 The PPy shell could prevent it from dissolution in aqueous electrolyte, but cannot completely
12 solve the dissolution problem. Therefore, the cycling stability is still not desirable due to the
13 interaction between V_2O_5 and aqueous electrolyte. To address this issue, replacing aqueous
14 electrolyte with gel electrolyte with very low moisture content can be one of solution to
15 improve the stability. Significantly, the LiNO_3/PVA gel electrolyte prominently improves the
16 stability of the device, with capacitance retention of 81.2% after 1000 cycles, because gel
17 electrolyte could prevent the chemical dissolution of vanadium oxides by minimizing the
18 water content, and avoid structure pulverization of vanadium oxides by holding the direct
19 contact between electrochemically active materials and substrate during cycling.³³
20 Furthermore, the cyclic stability of the as-prepared device stands in sharp in contrast to 48.8%
21 of capacitance loss for the supercapacitor based on V_2O_5 network. The improved stability is
22 due to fact that the PPy shell coated on the V_2O_5 nanowires prevents vanadium dissolution
23 into the electrolyte. To further assess the application value of the 3D $\text{V}_2\text{O}_5/\text{PPy}$ core/shell
24 network, we assembled supercapacitors, and charged it for only 10 s to $\sim 2 \text{ V}$, the devices
25 could power red light-emitting diode (LED) (5 mm diameter 1.8 V, 20 mA) indicators
26 efficiently (Fig. 4F).

1
2
3
4
5
6
7
8
9
10
11
12
13
14
15
16
17
18
19
20
21
22
23
24
25
26

Conclusions

The fabrication of the 3D V₂O₅/PPy interconnected core/shell network nanostructures has been developed with excellent capacitive performance of 448 F g⁻¹ arising from the synergetic effect from the V₂O₅ network and conductive PPy shell. The continuous 3D V₂O₅/PPy network creates channels for better ion transport, and the PPy shell could effectively enhance the electronic conductivity and prevent the dissolution of vanadium. Two-electrode symmetric supercapacitor based on V₂O₅/PPy core/shell network electrodes further delivers high specific energy and power densities, as well as exhibits outstanding cycling life. Furthermore, the simple and cost-effect assembly of the supercapacitor electrodes illustrate potential applications for small warning light, clock chip, and wearable electronics.

Acknowledgements

We acknowledge the support from the "Thousand Talents Program", the Natural Science Foundation of Jiangsu Province of China (no. BK20140315), the National Natural Science Foundation of China (no. 51402202), the National Basic Research Program of China (no. 2015CB358600), Jiangsu shuangchuang plan, and the Priority Academic Program Development of Jiangsu Higher Education Institutions (PAPD).

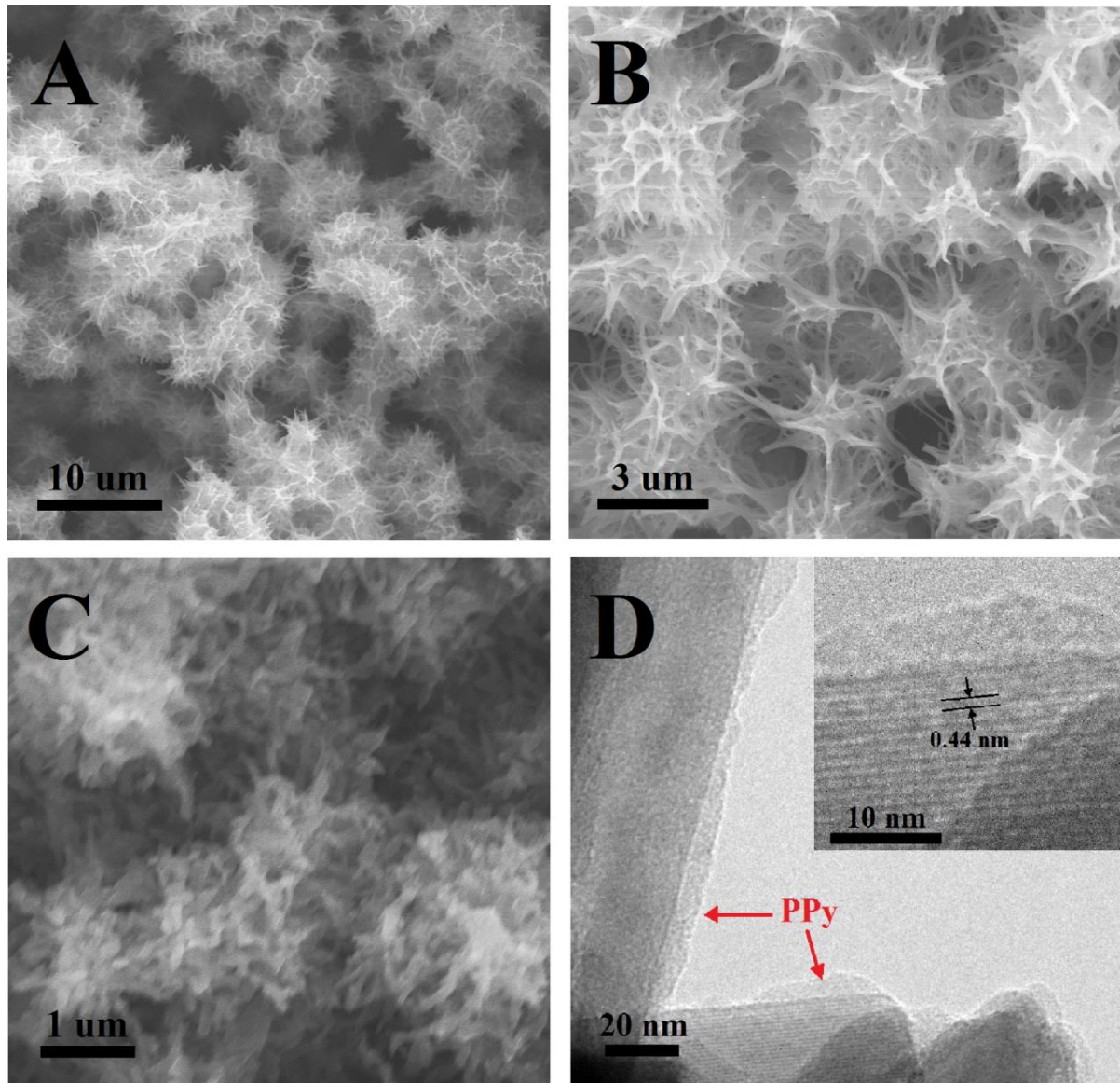
Notes and references

- 1 S. D. Perera, A. D. Liyanage, N. Nijem, J. P. Ferrarus, Y. J. Chabal and K. J. Balkus, *J. Power Sources*, 2013, **230**, 130.
- 2 D. Choi, G. E. Blomgren and P. N. Kumta, *Adv. Mater.*, 2006, **18**, 1178.
- 3 Y. W. Zhu, S. Murali, M. D. Stoller, K. J. Ganesh, W. W. Cai, P. J. Ferreira, A. Pirkle, R. M. Wallace, K. A. Cychosz, M. Thommes, D. Su, E. A. Stach and R. S. Ruoff, *Science*, 2011, **332**, 1537.

- 1 4 M. L. Li, G.Y. Sun, P. P. Yin, C. P. Ruan and K. Ai, *ACS Appl. Mater. Interfaces*, 2013, **5**,
2 11462.
- 3 5 G. P. Wang, L. Zhang and J. J. Zhang, *Chem. Soc. Rev.*, 2012, **41**, 797.
- 4 6 C. Y. Foo, A. Sumboja, D. J. H. Tan and J. H. Wang, P. S. Lee, *Adv. Energy Mater.*, 2014,
5 **10**, 1002.
- 6 7 C. C. Hu, W. C. Chen and K. H. Chang, *J. Electrochem. Soc.*, 2004, **151**, A281.
- 7 8 J. Yan, E. Khoo, A. Sumboja and P. S. Lee, *ACS Nano*, 2010, **4**, 4247.
- 8 9 Z. S. Wu, W. C. Ren, L. Wen, L. B. Gao, J. P. Zhao, Z. P. Chen, G. M. Zhou, F. Li and H.
9 M. Cheng, *ACS Nano*, 2010, **4**, 3187.
- 10 10 J. W. Lang, L. B. Kong, W. J. Wu, Y. C. Luo and L. Kang, *Chem. Commun.*, 2008, **35**,
11 4213.
- 12 11 A. M. Glushenkov, D. Hulicova-Jurcakova, D. Llewellyn, G. Q. Lu and Y. Chen, *Chem.*
13 *Mater.*, 2010, **22**, 914.
- 14 12 X. H. Lu, M. H. Yu, T. Zhai, G. M. Wang, S. L. Xie, T. Y. Liu, C. L. Liang, Y. X. Tong
15 and Y. Li, *Nano Lett.*, 2013, **13**, 2628.
- 16 13 G. D. Nie, X. F. Lu, J. Y. Lei, Z. Q. Jiang and C. Wang, *J. Mater. Chem. A*, 2014, **2**, 15495.
- 17 14 S. Boukhalifa, K. Evanoff and G. Yushin, *Energy Environ. Sci.*, 2012, **5**, 6872.
- 18 15 Q. T. Qu, Y. S. Zhu, X. W. Gao and Y.P. Wu, *Adv. Energy Mater.*, 2012, **2**, 950.
- 19 16 Y. S. Hu, X. Liu, J. O. Muller, R. Schlogl and J. Maier, D. S. Su, *Angew. Chem. Int. Ed.*,
20 2009, **48**, 210.
- 21 17 A. Q. Pan, J. G. Zhang, Z. M. Nie, G. Z. Cao, B. W. Arey, G. S. Li, S. Q. Liang and J. Liu,
22 *J. Mater. Chem.*, 2010, **20**, 9193.
- 23 18 A. Q. Pan, H. B. Wu, L. Zhang and X. W. Lou, *Energy Environ. Sci.*, 2013, **6**, 1476.
- 24 19 Z. Chen, Y. C. Qin, D. Weng, Q. F. Xiao, Y. T. Peng, X. L. Wang, H. X. Li, F. Wei and Y.
25 F. Lu, *Adv. Funct. Mater.*, 2009, **19**, 3420.

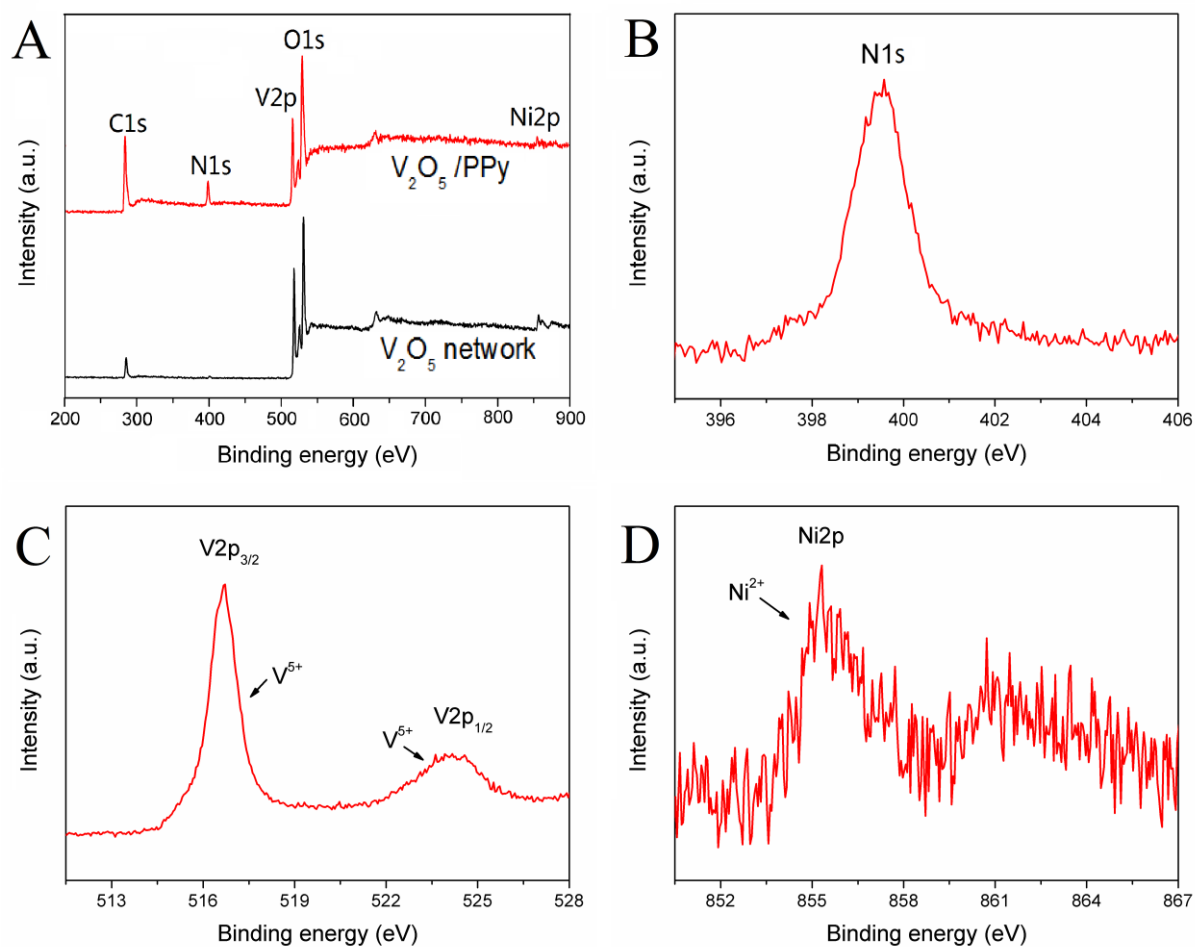
- 1 20 Z. Chen, V. Augustyn, J. Wen, Y. W. Zhang, M. Q. Shen, B. Dunn and Y. F. Lu, *Adv.*
2 *Mater.*, 2011, **23**, 791.
- 3 21 S. D. Perera, B. Patel, N. Nijem , K. Roodenko , O. Seitz , J. P. Ferraris ,Y. J. Chabal and
4 K. J. Balkus, *Adv. Energy. Mater.*, 2011, **1**, 936.
- 5 22 Y. Yang, L. Li, H. L. Fei, Z. W. Peng, G. D. Ruan and J. M. Tour, *ACS Appl. Mater.*
6 *Interfaces*, 2014, **6**, 9590.
- 7 23 C. Zhou, Y. W. Zhang, Y. Y. Li and J. P. Liu, *Nano Lett.*, 2013, **13**, 2078.
- 8 24 T. Qian, C. F. Yu, S. S. Wu and J. Shen, *J. Mater. Chem. A*, 2013, **1**, 6539.
- 9 25 T. Qian, X. Zhou, C. F. Yu, S. S. Wu and J. Shen, *J. Mater. Chem. A*, 2013, **1**, 15230.
- 10 26 J. Y. Ji, L. L. Zhang, H. X. Ji, Y. Li, X. Zhao, X. Bai, X. B. Fan, F. B. Zhang and R. S.
11 Ruoff, *ACS Nano*, 2013, **7**, 6237.
- 12 27 M. J. Deng, C. C. Wang, P. J. Ho, C. M. Lin, J. M. Chen and K. T. Lu, *J. Mater. Chem. A*,
13 2014, **10**, 1039.
- 14 28 J. X. Zhu, L. J. Cao, Y. S. Wu, Y. J. Gong, Z. Liu, H. E. Hoster, Y. H. Zhang, S. T. Zhang, S.
15 B. Yang, Q. Y. Yan, P. M. Ajayan and B. Vajtai, *Nano Lett.*, 2013, **13**, 5408.
- 16 29 P. H. Yang, X. Xiao, Y. Z. Li, Y. Ding, P. F. Qiang, X. H. Tan, W. J. Mai, Z. Y. Lin, W.Z.
17 Wu, T. Q. Li, H. Y. Jin, P. G. Liu, J. Zhou, C. P. Wong and Z. L. Wang, *ASC Nano*, 2013, **7**,
18 2617.
- 19 30 B. Saravanakumar, K. K. Purushothaman and G. Muralidharan, *ACS Appl. Mater.*
20 *Interfaces*, 2012, **4**, 4484.
- 21 31 Y. Yang, S. P. Albu, D. Kim and P. Schmuki, *Angew. Chem.*, 2011, **123**, 9237.
- 22 32 Y. Yang, D. Kim, M. Yang and P. Schmuki, *Chem. Commun.*, 2011, **47**, 7746.
- 23 33 G. Wang, X. Lu, Y. Ling, T. Zhai, H. Wang, Y. Tong and Y. Li, *ACS Nano*, 2012, **6**, 10296.
- 24 34 A. Bahloul, B. Nessark, E. Briot, H. Groult, A. Mauger, K. Zaghbi and C. M. Julien, *J.*
25 *Power Sources*, 2013, **240**, 267.
- 26 35 K. B. Hatzell, L. Fan, M. Beidaghi, M. Boota, E. Pomerantseva, E. C. Kumbur and Y.

- 1 Gogotsi, *ACS Appl. Mater. Interfaces*, 2014, **6**, 8886.
- 2 36 Z. S. Wu, W. C. Ren, D. W. Wang, F. Li, B. L. Liu and H. M. Cheng, *ACS Nano*, 2010, **10**,
- 3 5835.
- 4 37 Y. M. He, W. J. Chen, X. D. Li, Z. X. Zhang, J. C. Fu, C. H. Zhao and E. Q. Xie, *ACS Nano*,
- 5 2013, **1**, 174.
- 6 38 Z. B. Lei, J. T. Zhang and X. S. Zhao, *J. Mater. Chem.*, 2012, **22**, 153.
- 7

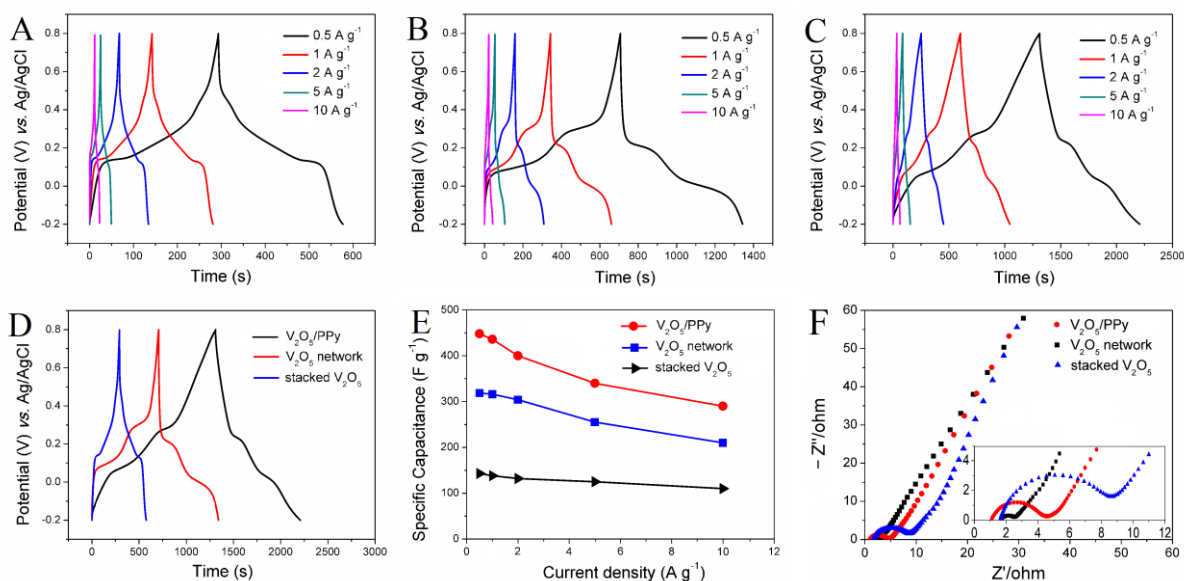


1
2 **Fig. 1** (A) Low-magnification and (B) high-magnification SEM images of the V₂O₅ network
3 (C) High-magnification SEM images of the V₂O₅/PPy core/shell network (D) HRTEM image
4 of the surface of V₂O₅/PPy core/shell network. Inset shows the V₂O₅ crystal lattice and
5 amorphous PPy structures.

6

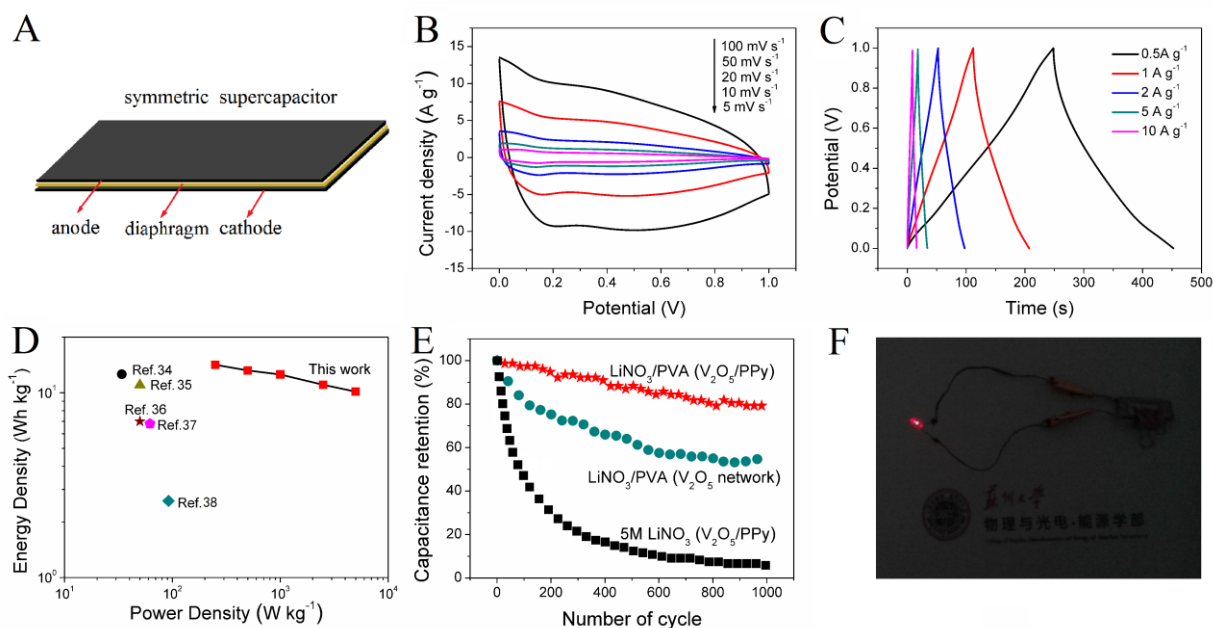


1
 2 **Fig. 2** (A) Full X-ray photoelectron spectroscopy (XPS) spectra of the V_2O_5 , and V_2O_5/PPy
 3 core/shell network. The high resolution (B) N1s, (C) V2p and (D) Ni2p XPS spectra.
 4

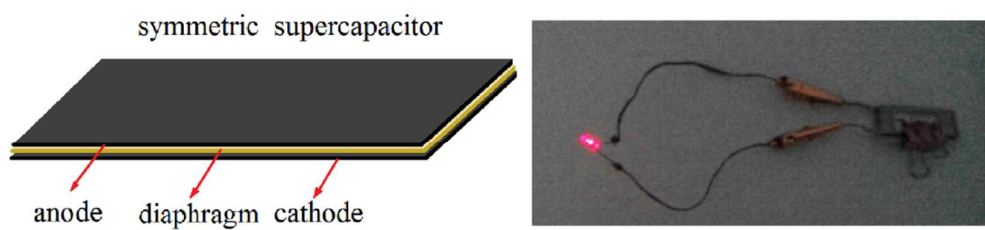


1
2 **Fig. 3** Galvanostatic charge/discharge curves of the prepared (A) stacked V₂O₅, (B) V₂O₅
3 network, and (C) V₂O₅/PPy core/shell network electrode at current densities of 0.5, 1, 2, 5, 10
4 A g⁻¹. (D) Galvanostatic charge/discharge curves of three different materials at a scan rate of
5 0.5 A g⁻¹. (E) Specific capacitances of three different materials at different current densities.
6 (F) Nyquist plots of the three prepared different materials electrodes.

7



1
 2 **Fig. 4** (A) Schematic illustration of the symmetric supercapacitor configuration. (B) CVs and
 3 (C) charge-discharge curves of the symmetric supercapacitor. (D) Ragone plots of the solid-
 4 state V_2O_5/PPy devices. The values reported for other devices are added for
 5 comparison.^{34,35,36,37,38} (E) Cycling performance of single V_2O_5/PPy electrode and symmetric
 6 V_2O_5/PPy device collected at the current density of $10A g^{-1}$ for 1000 cycles in 5 M $LiNO_3$
 7 aqueous solution and $LiNO_3/PVA$ gel electrolyte, respectively. (F) A picture showing that the
 8 supercapacitor can lighten up a LED indicator.



We reported all-solid-state supercapacitors based on interconnected three-dimensional V_2O_5 /polypyrrole network nanostructures with enhanced pseudocapacitive performance.